JPEDAV (2004) 25:355-363
DOI: 10.1361/15477030420124
1547-7037/$19.00 ©ASM International



# Contribution to the Zr-Rich Part of the Zn-Zr Phase Diagram

*Maureen E. Williams, William J. Boettinger, and Ursula R. Kattner*

*(Submitted September 10, 2003; in revised form April 16, 2004)*

**The reaction of zinc vapor with Zircaloy-4 and nuclear grade zirconium was investigated with various analytical techniques: optical metallography, scanning electron microscopy (SEM), and transmission electron microscopy (TEM). Based on the results, the Zr-rich part of the Zn-Zr phase diagram was revised. A eutectoid decomposition of (βZr) occurs at 718 ± 6 °C with a composition of $x_{Zr}$ = 0.865; this temperature is lower than the previously accepted 750 °C eutectoid. The solubility of Zn in (αZr) was determined to be at $x_{Zn}$ = 0.0236, a maximum at 725 °C. The intermetallic phase $ZnZr_2$ was observed to occur in samples heat treated at 712 °C and 725 °C, but not in those heat treated at 700 °C and 775 °C.**

## 1. Introduction

Spent nuclear fuel storage in the United States is a major concern for both the power utilities that operate nuclear power plants and the government regulating authority, the Nuclear Regulatory Commission (NRC). Due to delays in the completion of permanent storage facilities, increased long-term reliability for temporary storage systems is required.

A current method for temporarily storing spent nuclear fuel is the so-called dry cask storage system (DCSS). When a spent fuel bundle, containing as many as 300 individual fuel rods, is removed from a reactor core, it is placed in a pool of water for approximately five years to radioactively "cool." The "cooled" fuel bundle is then loaded underwater (to limit radioactive exposure) into a steel storage container called a cask. After loading is completed, the cask is removed from the water, vacuum dried, and the top sealed by welding. The internal temperature of the DCSS is expected to equilibrate at approximately 350 °C during normal dry storage. However, the maximum internal temperature may reach 570 °C during vacuum drying.[1] The DCSS containing this spent fuel is stored until a permanent storage facility is available.

In recent years, the practice of coating the inside of the DCSS with zinc (Zn) paint has been implemented to prevent corrosion. However, there is a possibility that Zn introduced into the sealed storage system could react with the fuel rod cladding material Zircaloy-4* [a zirconium (Zr) alloy containing small amounts of tin (Sn), iron (Fe), and chromium (Cr)],[2] and form Zn-Zr intermetallics [the solubility of Zn in (αZr) is very small]. If the reaction layer between the Zircaloy-4 and Zn vapor given off by the paint during storage at 350 °C is large enough to degrade the fuel cladding and cause cracks or gross ruptures during the dry storage, then the transfer of the spent fuel in the casks to the permanent repository may not be possible without a costly repackaging of the spent fuel.[3]

To better understand the reaction of Zn vapor with Zircaloy-4, experiments using both Zircaloy-4 and nuclear grade Zr exposed to Zn vapor from α-brass (Cu-30 ms. %† Zn) were conducted at temperatures up to 800 °C.[4] α-brass was used instead of pure Zn as a vapor source to better approximate the vapor pressure of the Zn in the paint. The Zn-Zr phase diagram, Fig. 1,[5] provides the basis for understanding the possible Zn reactions with nuclear grade Zr and its alloys. However, the Zn-Zr binary system is not well defined on the Zr-rich side, as indicated by the dashed lines on phase diagram. The present paper describes the reactions and kinetics observed between Zr and Zn vapor at temperatures above 650 °C.

## 2. The Zn-Zr System

The available experimental information for the Zn-Zr system was evaluated by Dutkiewicz.[5] The phase diagram accepted in that evaluation is shown in Fig. 1. In addition to the three terminal solid solutions, eight intermetallic phases[5,6] have been reported for this system. Lattice parameters, space groups, and structure prototypes of these phases are listed in Table 1. Three intermetallic phases, $Zn_{22}Zr$, $Zn_2Zr_3$, and $ZnZr_2$ are not shown in the accepted Zn-Zr phase diagram. A large solubility of Zn in (βZr) and negligible solubility for Zn in (αZr) have been estimated in the Dutkiewicz phase diagram, although no data are reported.

The invariant reactions of the condensed phases of the Zn-Zr system are summarized in Table 2.[5] The two reac-

**Maureen E. Williams, William J. Boettinger,** and **Ursula R. Kattner,** Metallurgy Division, National Institute of Standards and Technology 100 Bureau Dr., Mailstop 8555, Gaithersburg MD 20899-8555. Contact e-mail: Maureen.Williams@nist.gov.

* Commercial equipment and materials are identified in order to adequately specify certain procedures. In no case does such identification imply recommendation or endorsement by the National Institute of Standards and Technology, nor does it imply that the materials or equipment identified are necessarily the best available for the purpose.

† The notation 'ms.%' is defined as 100 % × W, where W is the mass fraction of an element in the alloy and the notation 'at.%' is defined as 100 % × N, where N is the molar fraction of an element in the alloy.

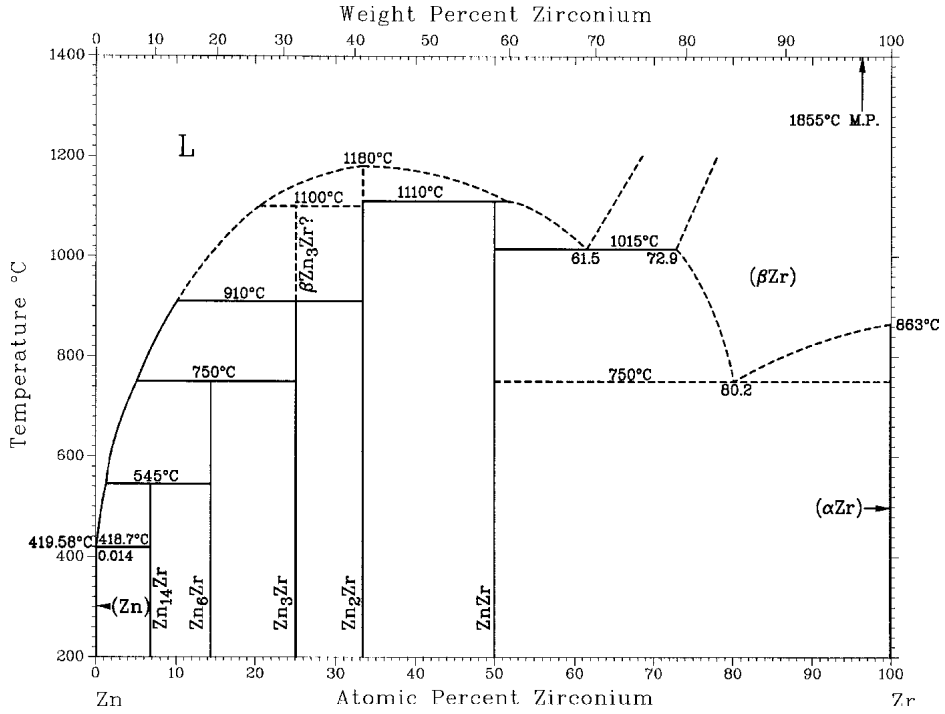


**Fig. 1** Zn-Zr phase diagram[5]

**Table 1 Composition, Lattice Parameters, Space Group, and Prototype of Phases in the Zn-Zr System[5,6]**

| Phase | Composition, at.% Zr | Lattice Parameter, nm | | | Space Group | Prototype |
|---|---|---|---|---|---|---|
| | | *a* | *b* | *c* | | |
| (Zn) | 0 | 0.2644 | … | 0.49494 | $P6_3/mmc$ | Mg |
| $Zn_{22}Zr$ (a) | … | 0.14103 | … | … | $Fd\bar{3}m$ | $Mg_3Cr_2Al_{18}$ |
| $Zn_{14}Zr$ | 6.67 | 0.1411 | … | … | $Fd\bar{3}m$ | $Mg_3Cr_2Al_{18}$ |
| $Zn_6Zr$ | 14.3 | 0.127 | … | 0.868 | … | … |
| $Zn_3Zr$ | 25 | 0.816 | … | 1.623 | … | … |
| $Zn_2Zr$ | 33.3 | 0.7396 | … | … | $Fd\bar{3}m$ | $Cu_2Mg$ |
| ZnZr | 50 | 0.3336 | … | … | $Pm\bar{3}m$ | CsCl |
| $Zn_2Zr_3$ (a) | 60.5 | 0.7633 | … | 0.6965 | $P4_2nm$ | $Al_2Gd_3$ |
| $ZnZr_2$ (a) | 66.7 | 0.3303 | … | 1.126 | $I4/mmm$ | $MoSi_2$ |
| (βZr) | 100 | 0.3609 | … | … | $Im\bar{3}m$ | W |
| (αZr) | 100 | 0.32317 | … | 0.51476 | $P6_3/mmc$ | Mg |

(a) Phase is not shown in the phase diagram, Figure 1.

**Table 2 Invariant Points of the Condensed Zn-Zr Binary Phase Diagram[5]**

| Reaction | Phase Compositions, at.% Zr | | | Temperature, °C | Reaction Type |
|---|---|---|---|---|---|
| L ↔ Zn | 0 | … | … | 419.58 | Melting |
| L ↔ (Zn) + $Zn_{14}Zr$ | 0.014 | 0.01 | 6.67 | 418.7 | Eutectic |
| L + $Zn_6Zr$ ↔ $Zn_{14}Zr$ | 1.1 | 14.3 | 6.67 | 545 | Peritectic |
| L + $Zn_3Zr$ ↔ $Zn_6Zr$ | 4.4 | 25.0 | 14.3 | 750 | Peritectic |
| L + $Zn_2Zr$ ↔ $Zn_3Zr$ | 10.0 | 33.3 | 25.0 | 910 | Peritectic |
| L ↔ $Zn_2Zr$ | 33.3 | … | … | 1180 | Congruent |
| L + $Zn_2Zr$ ↔ ZnZr | 51.8 | 33.3 | 50 | 1110 | Peritectic |
| L ↔ ZnZr + (β–Zr) | 61.5 | 50 | 73 | 1015 | Eutectic |
| (βZr) ↔ ZnZr + (αZr) | 80.2 | 50 | 100 | 750 | Eutectoid |
| L ↔ βZr | 100 | … | … | 1855 | Melting |
| βZr ↔ αZr | 100 | … | … | 863 | Allotropic |

tions of interest for the present work are the allotropic transformation of Zr and the eutectoid reaction. Elemental Zr undergoes an allotropic phase transformation at 863 °C from high temperature βZr with bcc structure to low temperature αZr with cph structure. On the Zr-rich side of the system, high temperature (βZr) transforms in a eutectoid reaction at 750 °C into (αZr) and the intermetallic ZnZr. However, Rossteutscher and Schubert[7] found the phase $ZnZr_2$ in samples together with (αZr) and ZnZr. This suggests that a metastable or stable eutectoid reaction, (βZr) → (αZr) + $ZnZr_2$, may occur. Hood[8] measured the diffusion of Zn in single crystal (αZr).

## 3. Experimental

### 3.1 Sample Preparation

The samples were prepared from nuclear grade Zr provided by Oremet-Wah Chang and Zircaloy-4 provided by McDermott Technology, Inc. The nuclear grade Zr contains less than 1000 parts per million (ppm) by mass of all trace elements including hafnium. Zircaloy-4 is a dilute Zr alloy containing 1.5 ms. % Sn, 0.2 ms.%Fe, and 0.1 ms.%Cr.[2]

The Zn vapor source used for this study was α-brass (Cu-30 ms.% Zn) that contains less than 0.01 ms.% Fe. A 12.7 mm diameter rod was cleaned with ethyl alcohol, and the rod was turned on a lathe to remove the surface layer. Thin brass filings were produced by further machining. The

**Table 3 Activity and Chemical Potential of Zn in α-brass (Cu-30 ms.% Zn, Reference State Liquid Zn)**

| Temperature, °C | Activity of Zn in α-Brass | Chemical Potential of Zn in α-Brass, J/mol | Vapor Pressure of Pure Zn, kPa | Partial Pressure of Zn over α-Brass, kPa |
|---|---|---|---|---|
| 650 | $5.1404 \times 10^{-2}$ | $-2.2781 \times 10^{4}$ | 3.59 | 0.185 |
| 670 | $5.5459 \times 10^{-2}$ | $-2.2679 \times 10^{4}$ | 4.98 | 0.276 |
| 700 | $6.1786 \times 10^{-2}$ | $-2.2527 \times 10^{4}$ | 7.85 | 0.485 |
| 712 | $6.4396 \times 10^{-2}$ | $-2.2466 \times 10^{4}$ | 9.44 | 0.608 |
| 725 | $6.7272 \times 10^{-2}$ | $-2.2399 \times 10^{4}$ | 11.4 | 0.767 |
| 775 | $7.8786 \times 10^{-2}$ | $-2.2145 \times 10^{4}$ | 22.48 | 1.771 |
| 800 | $8.4792 \times 10^{-2}$ | $-2.2017 \times 10^{4}$ | 30.83 | 2.614 |

**Table 4(a) Phase Sequence of Nuclear Grade Zirconium after Heat Treatment in Zinc Vapor**

| Temperature, °C | Time, days | Phase Sequence | ID |
|---|---|---|---|
| 650 | 16 | $Zn_2Zr$, ZnZr, (αZr) | 1 |
| | 64 | $Zn_2Zr$, ZnZr, (αZr) | 1 |
| 700 | 12 | $Zn_2Zr$, ZnZr, (αZr) | 1 |
| | 32 | $Zn_2Zr$, ZnZr, (αZr) | 1 |
| 712 | 11.8 | $Zn_2Zr$, ZnZr, $ZnZr_2$, (αZr) | 2 |
| 725 | 11.8 | $Zn_2Zr$, ZnZr, $ZnZr_2$, (βZr), (αZr) | 3 |
| | 12 | $Zn_2Zr$, ZnZr, $ZnZr_2$, (βZr), (αZr) | 3 |
| | 64 | $Zn_2Zr$, ZnZr, $ZnZr_2$, (βZr), (αZr) | 3 |
| 775 | 12 | ZnZr, (βZr), (αZr) | 4 (a) |
| 800 | 12 | ZnZr, (βZr), (αZr) | 4 (a) |

Note: The 65-70 at.% Zr phase, $ZnZr_2$, develops as a single phase layer.
(a) Same sequence as 2 or 4 except for the surface phase, $Zn_2Zr$, which could not be detected.

**Table 4(b) Phase Sequence of Zirclaoy-4 after Heat Treatment in Zinc Vapor**

| Temperature, °C | Time, days | Phase Sequence | ID |
|---|---|---|---|
| 650 | 16 | $Zn_2Zr$, (Zn)Zr, {(Zn)Zr + (Zn)$Zr_2$}, (αZr) | 2 |
| | 64 | $Zn_2Zr$, (Zn)Zr, {(Zn)Zr + (Zn)$Zr_2$}, (αZr) | 2 |
| | 126 | $Zn_2Zr$, (Zn)Zr, {(Zn)Zr + (Zn)$Zr_2$}, (αZr) | 2 |
| 670 | 21 | $Zn_2Zr$, (Zn)Zr, {(Zn)Zr + (Zn)$Zr_2$}, (αZr) | 2 |
| 700 | 4 | $Zn_2Zr$, (Zn)Zr, {(Zn)Zr + (Zn)$Zr_2$}, (αZr) | 2 |
| 700 | 10 | (Zn)Zr, {(Zn)Zr + (Zn)$Zr_2$}, (αZr) | 2 (a) |
| | 32 | $Zn_2Zr$, (Zn)Zr, {(Zr)Zr + (Zn)$Zr_2$}, (αZr) | 2 |
| 725 | 2 | $Zn_2Zr$, (Zn)Zr, (βZr), (αZr) | 4 |
| | 11.8 | (Zn)Zr, (Zn)$Zr_2$, (βZr), (αZr) | 5 |
| | 39 | (Zn)Zr, (βZr), (αZr) | 4 (a) |

Note: The 65-70 at.% Zr phase formed as a two phase layer of (Zn)Zr + (Zn)$Zr_2$.
(a) Same sequence as 2 or 4 except for the surface phase, $Zn_2Zr$, which could not be detected.

brass filings were cleaned in an ultrasonic bath with acetone and ethyl alcohol and stored in a desiccator.

The Zircaloy-4 and the nuclear grade Zr samples were sliced from bulk material with a diamond saw. All samples were cut to approximately the same dimensions, 12 mm long, 3 mm wide, and 1.5 mm thick. The surfaces were ground, finishing with wet 600 grit SiC paper, and then polished with a 6 μm diamond suspension. The samples were then cleaned with acetone and ethanol and air dried. Samples were vacuum encapsulated, using a diffusion pump system, in a quartz tube with a vacuum of $1.33 \times 10^{-5}$ Pa. The samples were annealed at approximately 700 °C for six days to relieve any stresses introduced by the fabrication process and sample preparation. After air cooling, the tube containing the annealed samples was broken and each sample was polished to 1/4 μm finish, cleaned, and then individually vacuum encapsulated, with the brass fillings with a vacuum of $1.33 \times 10^{-5}$ Pa. The sample and brass filings were separated by a quartz spacer. The Zn vapor pressure at the various heat treatment temperatures was calculated from the thermodynamic description of the Cu-Zn system[9] and is listed in Table 3. At the highest experimental temperature of 800 °C, the Zn vapor pressure over brass is 2.614 kPa and the vapor pressure of copper at 800 °C is insignificant.

In addition, a nuclear grade Zr sample to exposed Zn vapor at 800 °C was prepared for transmission electron microscope (TEM) analysis. This sample was ground with 600 grit SiC paper and then jet-electropolished with 5% perchloric acid and 95% ethanol with 35 V at a temperature of −5 °C.

### 3.2. Heat Treatment

A 50 mm inside diameter vertical Marshall tube furnace was used for the heat treatments. A nichrome cylindrical container, 82.5 mm tall with a 37.5 mm inside diameter, with a lid, was placed in the middle of the furnace hot zone and allowed to equilibrate to the furnace temperature. This produced an isothermal hot zone within the container. The furnace tube above and below the container was packed with firebrick to prevent convection currents in the tube. The encapsulated sample was placed inside the nichrome container. The sample was monitored by a type K (chromel-alumel) sheathed thermocouple placed through the lid to within 5 mm of the sample. This thermocouple was connected to a large external aluminum isothermal plate that serves as the cold junction reference. This external panel was connected to a temperature data acquisition board in a computer. The furnace temperature was maintained with a

separate type K thermocouple connected to a temperature controller. A three-point calibration, the melting points of lead (327 °C), Zn (419 °C), and aluminum (660 °C), was carried out for each of the thermocouples.

The samples were heat treated at 650 °C, 670 °C, 700 °C, 712 °C, 725 °C, 775 °C, and 800 °C for various lengths of time (Tables 4a, 4b). The initial choice of temperatures for the experiments was based on the Zn-Zr binary phase diagram (Fig. 1). Temperatures just below 750 °C were chosen to avoid the (βZr) phase, yet high enough to ensure that reaction would occur in the shortest period of time possible. However, experiments at 725 °C indicated the presence of (βZr), so additional experiments with nuclear grade Zr at temperatures above 725 °C were performed to confirm the eutectoid reaction temperature in the binary phase diagram.

At the end of the diffusion anneal the samples were quenched in water at room temperature. The sample was immersed in the water and then the quartz tube was broken using a hammer. The time from removal of the sample from the furnace until the quartz tube was broken underwater was approximately 5-10 s.

### 3.3 Characterization

All of the samples were cut in cross section and mounted in epoxy resin for optical metallography. The samples were then ground with 400 and 600 grit wet SiC papers and then polished starting with 15 μm diamond suspension and finishing with 0.25 μm diamond suspension.

Each sample was examined with a JEOL (Tokyo, Japan)

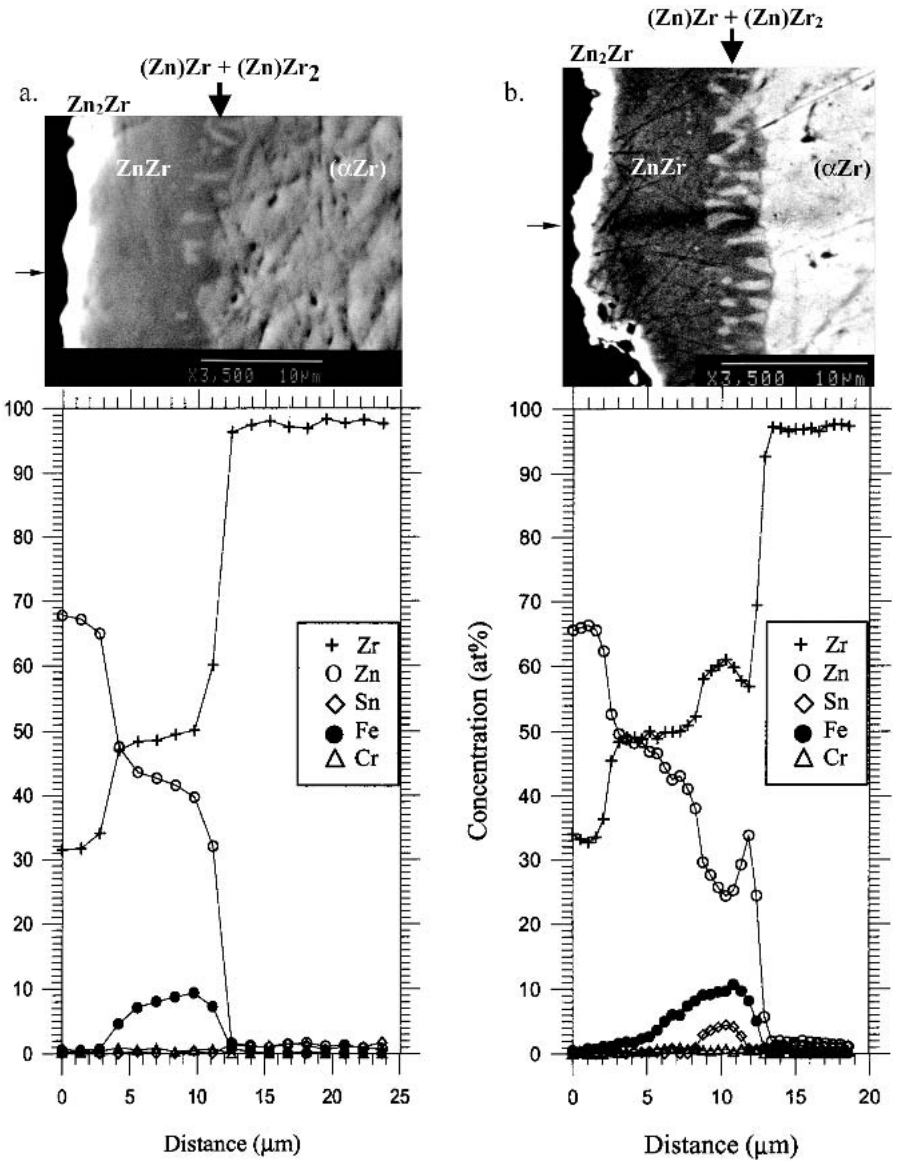


**Fig. 2** Zircaloy-4 exposed to Zn vapor at 650 °C for 126 d. The horizontal arrow indicates the path of the line scan, **(a)** the profile when the beam only passes through the matrix phase of the two-phase layer and **(b)** the profile when the beam passes through the precipitate phase of the two-phase layer. Note: the white region in the image is an edge effect from the electron beam.

model 840A scanning electron microscope (SEM). Using energy dispersive spectrometry (EDS), Noran System (Middleton, WI) 5500, with elemental standards for Zn, Zr, Sn, Fe, and Cr, a compositional line scan was done on each sample. All line scans were performed with an accelerating voltage of 20 kV, a probe current of 535 pA, and a 100 s acquisition time per point. The EDS composition profiles started at the edge of the sample and the electron beam was scanned toward the middle. The SEM electron beam resolution for EDS analysis is ~1 μm and the line scan steps were varied from 0.5 μm to 1.5 μm. The results gave a composition profile and the penetration depth of the Zn diffusion reaction zone.

The interpretation of the composition line scans was complicated by the multicomponent nature of Zircaloy-4. That is, only the Zr concentrations correspond to the ideal intermetallic stoichiometry and Fe and Sn atoms apparently substitute on Zn sites. Another complication was the formation of a two-phase layer of light colored precipitates in a dark colored matrix between two single-phase layers, Fig. 2. The white region along the edge is an "edge effect" from the electron beam. Phases identified in this line scan as (Zn, Fe, Sn)Zr (dark matrix) and (Zn, Fe, Sn)$Zr_2$ (light precipitate) are therefore designated as (Zn)Zr and (Zn)$Zr_2$, respectively. As the line scan crossed this layer, the beam was either overlapping the two phases, measuring an average composition of the precipitates and the matrix, or the beam hit only one phase and measured the precipitate or the matrix individually. Therefore the line scans across this two-phase layer do not give accurate compositions and individual point measurements were done on each of the phases in this two-phase layer separately.

## 4. Results

### 4.1 Line Scan Results

Tables 4(a) and 4(b) provide a summary the phase sequence of each individual nuclear grade Zr and Zircaloy-4 sample. Five distinct phase sequences were observed from the sample surface to the interior in nuclear grade Zr and Zircaloy-4 exposed to Zn vapor depending on temperature. To easily distinguish identical phase sequences, each sequence listed in Tables 4(a) and 4(b) is identified by a number.

The observed intermetallic phase growth due to Zn vapor reaction with the Zircaloy-4 and nuclear grade Zr generally agrees with the phases reported for the Zn-Zr system (Table 1). $Zn_2Zr$ is the first intermetallic to form on the surface of most of the samples. The ZnZr phase is present in all samples, and the $Zn_2Zr_3$ phase was not observed in any of the samples. A single phase layer of $ZnZr_2$ was found only in samples of nuclear grade Zr heat treated at 712 °C for 11.8 d, at 725 °C for 11.8 d, 12 d, and 64 d, and Zircaloy-4 at 725 °C for 11.8 d. The two-phase (Zn)Zr + (Zn)$Zr_2$ layer is only present in the multicomponent Zircaloy-4 samples heat treated at 650, 670, and 700 °C. The average composition of the individual phases in this two-phase layer, the matrix and precipitate, was determined by measuring four different points in each phase. The compositions of the matrix (Zn)Zr and precipitates (Zn)$Zr_2$ are listed in Table 5. The amount of growth of the two-phase layer can vary with location across the sample as shown in Fig. 3. In a binary diffusion couple of nuclear grade Zr exposed to Zn vapor a two-phase layer cannot form according to the Gibbs phase rule.[10]

In all the Zircaloy-4 and nuclear grade Zr samples that were exposed to Zn vapor at temperatures of 725 °C or higher, a (βZr) layer is present. The (Zn)$Zr_2$ or the (Zn)Zr + (Zn)$Zr_2$ two phase layer was observed in Zircaloy-4 samples that were heat treated at 725 °C for 2 d or 11.8 d or at lower temperatures but not in a Zircaloy-4 sample that was heat treated for 39 d at 725 °C. In the nuclear grade Zr samples only the 64 d 725 °C sample has the $ZnZr_2$ layer. The $ZnZr_2$ phase is absent in other nuclear grade Zr samples heat treated at 775 and 800 °C for 12 d.

### 4.2 Transmission Electron Microscopy of the β Phase

To confirm that phase labeled β was indeed a bcc structure, TEM analysis was performed. At 725 °C, below the reported eutectoid temperature of 750 °C, a (βZr) phase containing approximately 85 at.% Zr was observed. This same (βZr) phase was found in nuclear grade Zr samples heat treated at 775 and 800 °C for 12 d. The 800 °C sample had the largest (βZr) phase thickness of approximately 450 μm. TEM analysis of this sample confirmed the presence of a bcc structure that had martensitically transformed during quenching. Figure 4(a) shows SEM backscattered image of the martensitic structure on the electropolished surface, and Fig. 4(b) shows the TEM bright field image of the martensite with different orientations of plate-like variants of (αZr)

**Table 5 Composition of the Phases in the Two-Phase Region of Zircaloy-4 Exposed to Zinc Vapor**

| | Composition, at.% | | | | |
|---|---|---|---|---|---|
| | Zr | Zn | Sn | Fe | Cr |
| Light region | | | | | |
| Average | 63.78 | 22.70 | 2.78 | 10.41 | 0.36 |
| Standard deviation | 4.20 | 4.63 | 0.51 | 0.19 | 0.15 |
| Dark region | | | | | |
| Average | 52.78 | 36.35 | 0.58 | 9.55 | 0.70 |
| Standard deviation | 0.51 | 0.90 | 0.18 | 0.50 | 0.10 |

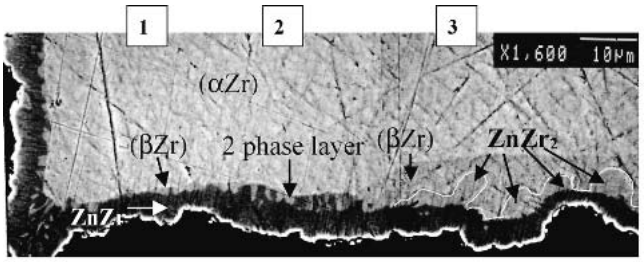


**Fig. 3** Zircaloy-4 exposed to Zn vapor at 725 °C for 11.8 d. Shown are three different phase sequences that are dependent on sample location 1, 2, and 3. (1) ZnZr, (βZr), (αZr), (2) ZnZr, two-phase layer of (Zn)Zr + (Zn)$Zr_2$, (βZr), (αZr), and (3) ZnZr, $ZnZr_2$, (βZr), (αZr) with the outline separating $ZnZr_2$ and (βZr).

expected for a quenched (βZr) phase. Figure 5 shows two selected TEM diffraction patterns from the large area of multiple variants from Fig. 4(b), a) pseudo three-fold symmetry with outlines of cph reciprocal lattices drawn over the pattern, and b) pseudo four-fold symmetry clearly corresponding to the parent bcc cubic phase. None of the samples below 725 °C contain the (βZr) phase (Table 4a and b), therefore, the phase observed in the diffusion experiments is the bcc (βZr).

### *4.3 Correction of the (βZr) Region in the Phase Diagram*

Compositional line scans of nuclear grade Zr exposed to Zn vapor at 712, 725, 775, and 800 °C are shown in Fig. 6. The sequence of phases is discussed in section 4.1. Although the ZnZr phase was present in all the samples, a clear plateau of the ZnZr phase in the Fig. 6(a) line scan is not apparent due to the resolution of the 1 μm diameter beam across the approximately 1 μm width of the ZnZr

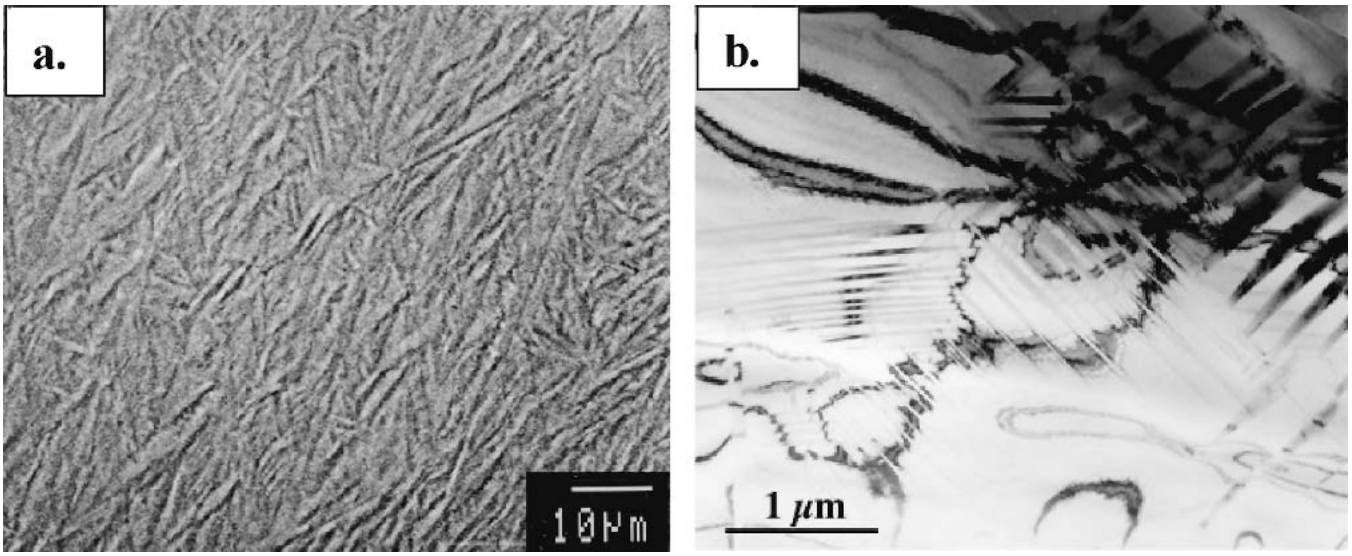


**Fig. 4** Nuclear grade Zr heat treated with Zn vapor at 800 °C. **(a)** SEM backscattered image of the martensitic structure, **(b)** TEM bright field image of the martensite with different orientations of the plate-like variants of (αZr)

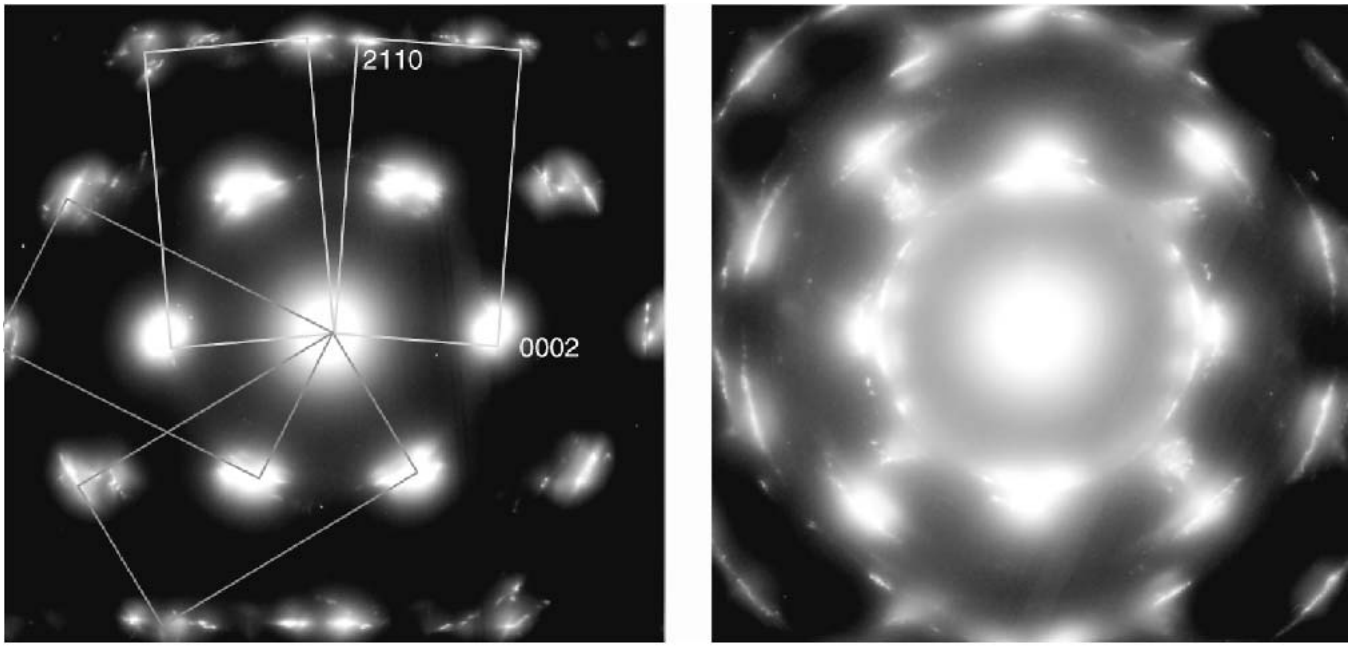


**Fig. 5** TEM diffraction patterns (a) and (b) are from the large area of multiple variants in Fig. 4(b) of nuclear grade Zr exposed to zinc vapor at 800 °C for 12 d. **(a)** three-fold symmetry and in **(b)** four-fold symmetry

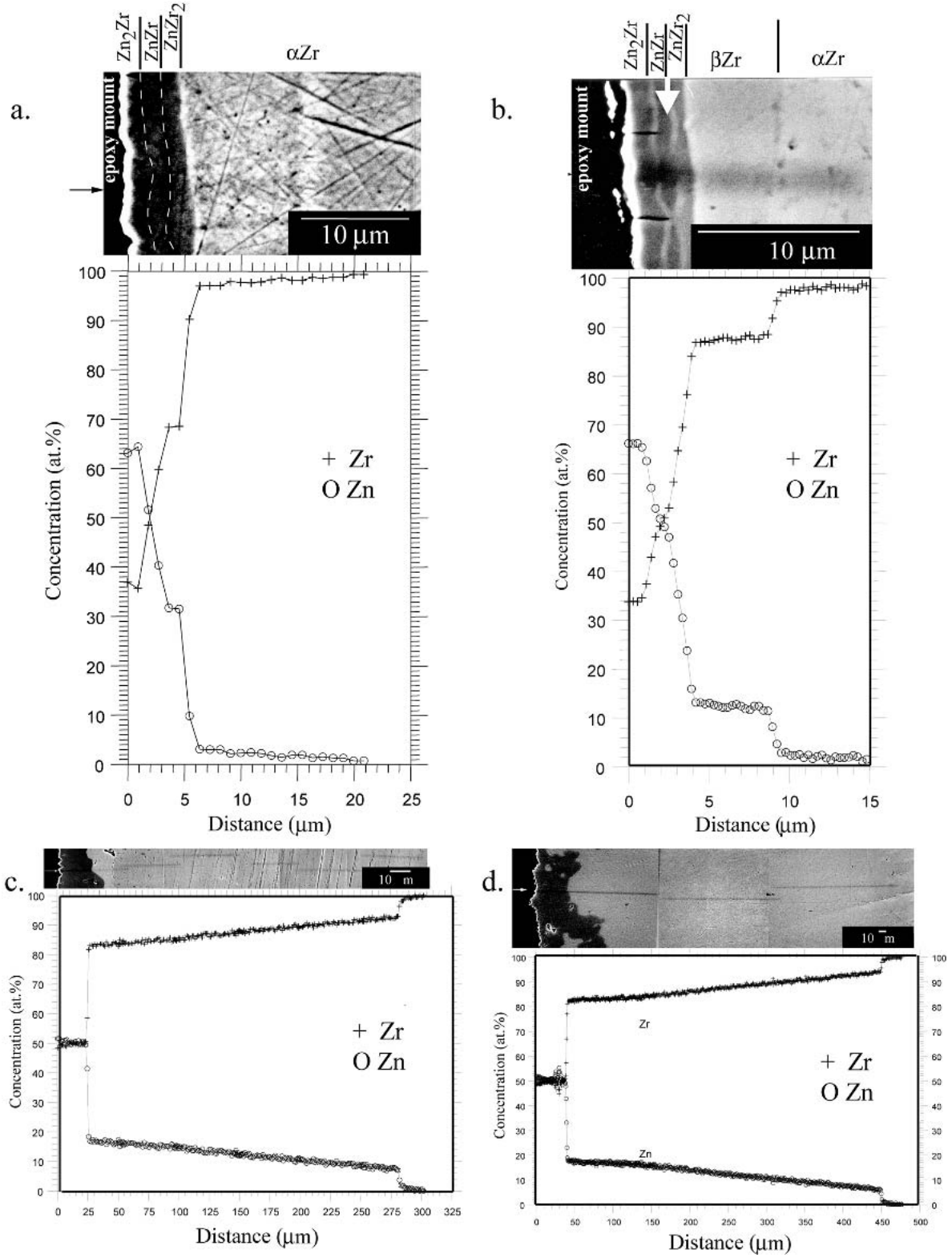


**Fig. 6** Nuclear grade Zr after heat treatment in Zn vapor and water quenching, **(a)** 712 °C for 11.8 d, **(b)** 725 °C for 11.8 d, **(c)** 775 °C for 12d, **(d)** 800 °C for 12 d.

phase. Also in the Fig. 6(b) line scan, the $ZnZr_2$ plateau is not apparent, but the phase is clearly visible in the micrograph. The (βZr) phase is not present at 712 °C, but is present at 725, 775, and 800 °C. The (βZr) phase, represented by a line with constant slope, ranges from 85-88 at.% Zr at 725 °C, 83.5-93 at.% Zr at 775 °C, and 82-95 at.% Zr

at 800 °C. The endpoints from each of these sloping lines determine the phase boundaries on both sides of the (βZr) homogeneity region above the eutectoid temperature. Figure 7 shows these experimental data points plotted with the currently reported phase diagram[5] in the region between 45 at.% Zr to 100 at.% Zr. The experimental results predict the eutectoid reaction temperature should be between 712 and 725 °C, so the temperature 718 °C was chosen as an estimate.

### 4.4 Solubility Estimate for (αZr)

Investigation of the nuclear grade Zr exposed to Zn vapor revealed a solubility of Zn in (αZr). Compositional line scan data of the nuclear grade Zr samples were acquired at different positions away from the surface until the amount of Zn in (αZr) reached zero and remained zero for approximately 5 μm. The total depth of Zn penetration into the nuclear grade Zr is reported in Table 6. The reported uncertainties in Table 6 are absolute bounds errors. The solubility limits were determined by extrapolating the measured values to the interface position. These data are listed in Table 6 and plotted in Fig. 7.

### 4.5 $ZnZr_2$ Phase

The $ZnZr_2$ phase was only observed in samples that were exposed to Zn vapor at temperatures of 712 and 725 °C. Assuming that no nucleation barriers exist, this suggests a phase diagram of the type shown in Fig. 7. A peritectoid reaction of (βZr) + ZnZr → $ZnZr_2$ should occur above 725 °C and a eutectoid reaction of $ZnZr_2$ → ZnZr + (αZr) below 712 °C. However, this temperature range could be larger, possibly from just above 700 °C to just below 775 °C. Another interpretation is that the $ZnZr_2$ fails to nucleate in the low temperature couples and that the $ZnZr_2$ phase exists down to much lower temperatures. Further work needs to be done to confirm the exact temperature range over which the $ZnZr_2$ phase exists.

**Table 6 Solubility Data of Zinc into Nuclear Grade α-Zirconium**

| Temperature, °C | Time, d | Reaction Zone Thickness, μm ± 0.5 μm | Total Penetration Depth of Zinc into (αZr), μm | Solubility of Zn in (αZr), at.% Zn ± 0.3 at.% |
|---|---|---|---|---|
| 650 | 16 | 3.0 | 18.0 | 0.76 |
| | 64 | 6.0 | 34.0 | NM |
| 700 | 12 | 3.2 | ~30.0 | NM |
| | 32 | 6.3 | ~70.0 | NM |
| 712 | 11.8 | 3.5 | 35.0 | 0.92 |
| 725 | 11.8 | 51.0 | 82.0 | 2.4 |
| | 64 | 205.0 | 265.0 | NM |
| 775 | 12 | 287.0 | ~300.0 | 2.2 |
| 800 | 12 | 450.0 | 465.0 | 1.2 |

(a) NM, Not measured.

## 5. Conclusions

Zircaloy-4 and nuclear grade Zr were exposed to Zn vapor in the temperature range of 650-800 °C. The spatial sequence of intermetallic phases from the surface into the interior and the total depth of Zn penetration were measured. The Zr-rich part of the Zn-Zr phase diagram was modified according to the results.

The eutectoid temperature was found to be lower than the currently reported temperature of 750 °C in the literature. The present work places the eutectoid reaction temperature at approximately 718 °C (±6 °C absolute bounds error) with a composition of 86.5 at.% Zr.

The solubility of Zn in nuclear grade α-Zr was measured from the composition line scan profiles at five different temperatures. The solubility of Zn increased with temperature from 0.76 at.% Zn at 650 °C to a maximum of 2.36 at.% Zn at 725 °C and decreased with further increases in temperature.

The intermetallic $ZnZr_2$ phase was observed to occur at 712 and 725 °C but not at 700 and 775 °C. Therefore, a peritectoid reaction, (βZr) + ZnZr → $ZnZr_2$ and a eutectoid reaction, $ZnZr_2$ → ZnZr + (αZr) occur between 700 and 775 °C.

### Acknowledgments

The authors thank Leonid Bendersky for the TEM work, John Manning for many inspiring discussions, and Charles Interrante, NRC, for technical discussions and support of the initial NIST study funded by the U.S. Nuclear Regulatory Commission, Rockville, MD, #AA7500015.

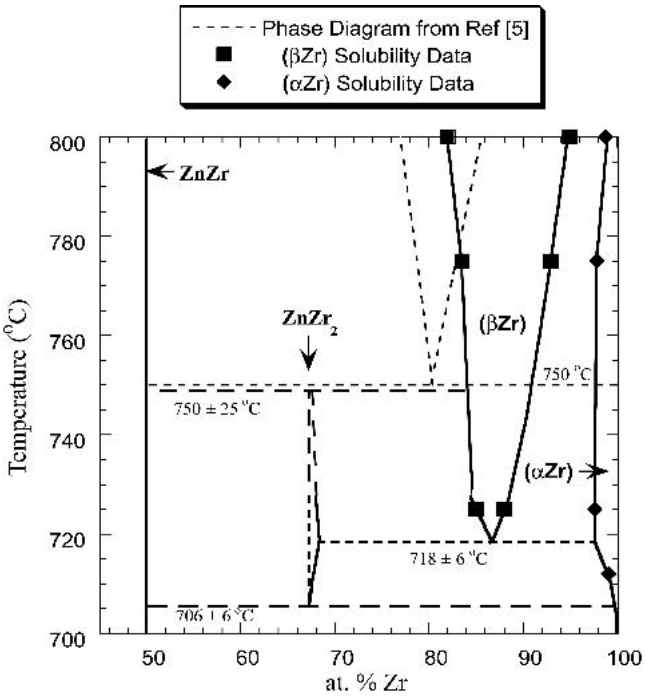


**Fig. 7** Revised Zr-rich part of the Zn-Zr phase diagram with experimental data from this study. The experimental error for the data is given in the text.

## References


1. Anon: NUREG-1536: "Standard Review Plan for Dry Cask Storage Systems: Section 4: Thermal Evaluation," NRC, Rockville, MD, Jan. 1997.
2. Anon: ASTM Standard B 350/B 350M, "Standard Specification for Zirconium and Zirconium Alloy Ingots for Nuclear Applications," *Annual Books of ASTM Standards,* Vol. 2.04, ASTM, West Conshohocken, PA, 2000, pp. 214-16.
3. Anon: NRC Bulletin 96-04, "Chemical, Galvanic, or other Reactions in Spent Fuel Storage and Transportation Casks," NRC, Rockville, MD, July 1996.
4. M.E. Williams: "The Reactions of Zinc Vapor with Zircaloy-4 and Pure Zirconium," NISTIR 6447, NIST, Gaithersburg, MD, Jan. 2000.
5. J. Dutkiewicz: "The Zn-Zr (Zinc-Zirconium) System," *J. Phase Equilibria,* 1992, *13*(4), pp. 430-33.
6. P. Villars and L.D. Calvert: *Pearson's Handbook of Crystallographic Data for Intermetallic Phases,* Vol. 4, 2nd ed., ASM International, Materials Park, OH, 1991, pp. 5364-65.
7. W. Rossteutscher and K. Schubert: "On Several T-Zn and T-Cd Alloy Systems," *Z. Metallkde.,* 1965, *56*(10), pp. 730-34 (in German).
8. G.M. Hood: "Solute Diffusion in α-Zr", *Diffusion Processes,* J.N. Sherwood, A.V. Chadwick, W.M. Muir, and F.L. Swinton, ed., Gordon and Breach, London, UK, 1971, pp. 361-72.
9. M. Kowalski and P.J. Spencer: "Thermodynamic Reevaluation of the Cu-Zn System," *J. Phase Equilibria,* 1993, *14,* pp. 432-8.
10. F.J.J. van Loo: "Multiphase Diffusion in Binary and Ternary Solid-State Systems," *Prog. Solid St. Chem.,* 1990, *20,* pp. 47-99.